Light Scattering and Microscopy from Block Copolymers with Cylindrical Morphology

M. C. Newstein, B. A. Garetz,* H. J. Dai, and N. P. Balsara*

Departments of Electrical Engineering, Chemistry, and Chemical Engineering, Polytechnic University, Brooklyn, New York 11201

Received December 14, 1994; Revised Manuscript Received April 14, 1995[⊗]

ABSTRACT: Cylindrical-morphology diblock copolymers, when ordered under quiescent conditions, exhibit a 4-fold cloverleaf H_V (depolarized) light scattering pattern, with an off-axis intensity maximum. The grain structure of these samples has been resolved by polarized-light microscopy. Closely-spaced grain pairs, whose optic axes are approximately perpendicular, have been observed. A correlated-grain-pair model is proposed, and scattering patterns are calculated using a correlation function approach. A 4-fold symmetry is a consequence of this model, and for some limited sets of model parameters, a qualitative agreement with experiment is observed.

I. Introduction

Block copolymers can self-assemble into a variety of ordered microstructures ranging from spherical and cylindrical dispersions to lamellar and bicontinuous cubic phases.[1] While considerable effort has been devoted to the characterization of the ordered microstructures and the order–disorder transitions,[1] relatively little is known about the extent of order in these materials. Ordered materials formed under quiescent conditions are globally disordered and contain a large number of imperfections. Coherent order is restricted to regions that are referred to as grains. Thomas and co-workers, using electron microscopy, have observed both discrete line and wall imperfections (defects and grain boundaries, respectively) as well as continuous changes in local microstructure orientation.[2] Actual grain shapes are highly irregular, and grain boundaries are not always well-defined. Many macroscopic properties of ordered block copolymer materials, such as elastic modulus[3] and order–disorder transition temperature,[4] depend on the size of these grains.

In some earlier work,[5,6] we showed how optical techniques could be used to probe the micron-scale grain structure of lamellar diblock copolymer materials. The angular distribution of the orthogonally-polarized scattered light from these materials can be related to a correlation function that describes the statistical properties of the grain structure. For randomly shaped grains with (1) a constant optic axis within a grain, (2) no correlation between grain shape and the direction of the grain optic axis, and (3) no correlation between the optic axes of different grains, we showed that the intensity pattern of the scattered light is azimuthally symmetric and peaked in the forward direction. The average grain size (length) was shown to be directly proportional to the total transmitted power and inversely proportional to the angular spread of the scattered beam. We were able to characterize, within this framework, the grain structures of several quiescently ordered lamellar diblock copolymer samples, prepared under a variety of annealing conditions.[5,6]

In this paper, we describe some recent work on polystyrene–polyisoprene diblock copolymer samples with cylindrical morphology. In these samples, the polyisoprene block is approximately 3 times longer than the polystyrene block, and the ordered morphology consists of hexagonally packed polystyrene cylinders in a polyisoprene matrix. These cylinders are approximately 8 nm in diameter with an intercylinder spacing of 16 nm,[7] and are thus not directly probed by optical methods. The medium, however, does exhibit local birefringence. Each region of coherently ordered cylinders behaves like a uniaxial birefringent crystallite with the optic axis parallel to the cylinder axis.[8] The depolarized light scattering patterns from these samples were found to be qualitatively different from the lamellar samples studied earlier.[5,6] In particular, the scattering patterns were not azimuthally symmetric, but cloverleaf shaped, with four intensity maxima at 45° from the polarizer/analyzer axes. Along these azimuthal maxima, the intensity profile had a maximum at a finite scattering angle (i.e., not in the forward direction). These features suggest the presence of correlations that were absent in the lamellar samples. Similar features have been observed in the light scattering from a wide range of materials, from crystalline polymers[9] to liquid crystals.[10]

We have also used polarized-light microscopy to characterize the block copolymer samples. There are several persistent features of samples we have studied. One is the appearance of a rectilinear texture oriented at 45° to the polarizer/analyzer axes. The other is the presence of bright grain pairs. Interposing a retarder tended to darken one or the other member of a pair, depending on retarder orientation, suggesting that these pairs have optic axes at approximately right angles to each other.

We have developed theoretical models that account for the observed scattering patterns and microscopy data, making the fewest assumptions possible. Correlations between shape and optic axes can lead to a scattering pattern with 4-fold symmetry. This may arise in cylindrical samples for a variety of reasons. For example, grain dimensions may tend to be longer in the direction parallel to the cylinder axis. However, a random collection of such grains would give a scattering pattern that peaks in the forward direction. To describe an intensity maximum at finite scattering angle, one must resort to a model in which the optic axis varies within the region of coherent order. Spherulites in crystalline polymers and nematic order in liquid crystalline polymers are modeled by very specific spatial

* To whom correspondence should be addressed.

[⊗] Abstract published in *Advance ACS Abstracts,* June 1, 1995.

0024-9297/95/2228-4587$09.00/0

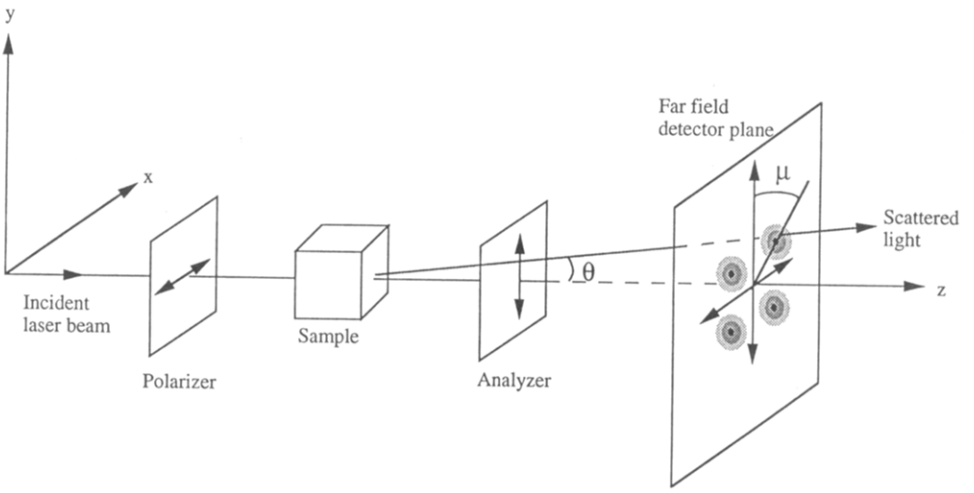

Figure 1. Schematic of experimental configuration.

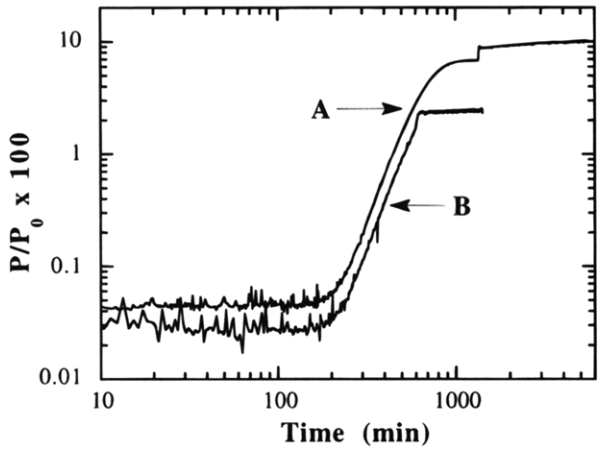

Figure 2. Transient birefringence signal vs time for tempering of SI(4-13) copolymer sample. Tempering time = 20 h for run A, 5 h for run B. log–log plot.

variations of the optic axis that are not appropriate for our block copolymer samples. A simple model that incorporates a varying optic axis, and one that is suggested by our polarized-light microscopy results, is a correlated-grain-pair (CGP) model, in which the region of coherence consists of a pair of grains, with a constant optic axis within each grain.

Correlations can be classified into correlations among pairs, triplets, and higher order combinations of decreasing importance. These high-order correlations become more important as the system becomes more ordered and eventually lead to the scattering maximum developing into a series of diffraction peaks. The light scattering pattern from a cylindrical block copolymer exhibits a single, relatively broad scattering peak. Thus, including only pair correlations is probably a good approximation. The assumption of uniform optic axis orientation within a grain is a simplification but was necessary to obtain a tractable solution. We have investigated the range of applicability of the CGP model in both two and three dimensions and find it a promising first step toward an understanding of correlations in the grain structure of diblock copolymers with cylindrical morphology.

II. Experimental Section

A. Polymer Synthesis. The polystyrene–polyisoprene diblock copolymer was synthesized by high-vacuum anionic polymerization, using *sec*-butyllithium as the initiator and methanol as the terminator. The polystyrene block was synthesized first, followed by the polyisoprene block. Both reactions were carried out at room temperature, in a 70/30 cyclohexane/benzene mixture. The block copolymer used in this study is designated SI(4-13), where the numbers in parentheses refer to the molecular weight in kg/mol of the polystyrene and polyisoprene blocks, respectively. DSC measurements at 10 °C/min in the temperature range from −25 to +100 °C revealed a glass transition at 51 °C. Details concerning the synthesis and characterization are given in ref 11.

B. Light Scattering Measurements. Small-angle light scattering measurements were performed on the apparatus depicted in Figure 1. A beam of light from a 15 mW helium–neon laser (wavelength = 632.8 nm) was directed through a horizontal Glan air-spaced prism polarizer, followed by the sample, which was immersed in a constant temperature, index-matching fluid bath. A compensator (quartz quarter-wave retardation plate) was inserted between the polarizer and sample. The light emerging from the sample passed through an analyzer (a vertical large-area dichroic polarizer), followed by a screen, camera, or photodetector mounted on a two-dimensional translation stage. The resultant far-field scattering pattern, commonly designated H_V or V_H, could be observed visually or photographically, or the intensity distribution could be measured point-by-point by translating a photodetector.

Samples were contained in sealed test tubes with a path length of 0.74 cm. SI(4-13) has an order–disorder transition temperature, $T_{ODT} = 58 \pm 1$ °C. Sample preparation involved first disordering the sample by heating it to 70 °C and then cooling it to 53.5 °C. The sample was tempered at 53.5 °C for a variable length of time and then quenched to 22 °C. The birefringence of the sample (as measured by P/P_0, where P_0 and P are the incident and transmitted powers, respectively) was monitored throughout the process by collecting the light exiting the analyzer and focusing it onto a photodiode with a large lens. The transient signal from the photodetector was recorded immediately after the sample was quenched to 53.5 °C from 70 °C.

Typical transient signal trajectories are shown in Figure 2. The transmitted power of two different runs, denoted as A and B, is plotted as a function of time on a log–log scale. In run A, the sample was tempered until the transient signal leveled off, and the tempering time was about 20 h. In run B, the tempering time was

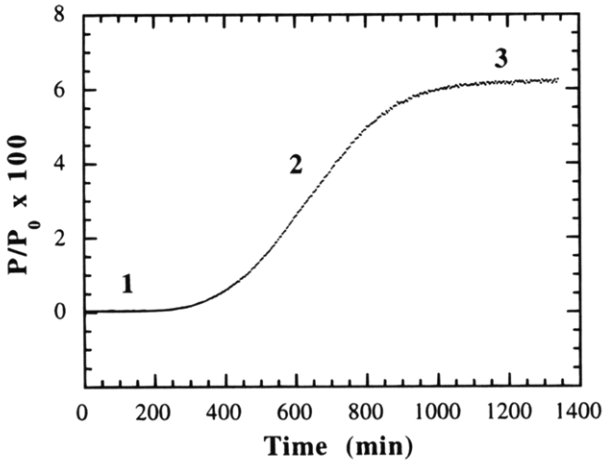

Figure 3. Tempering trajectory for run A. Linear plot, times < 1400 min.

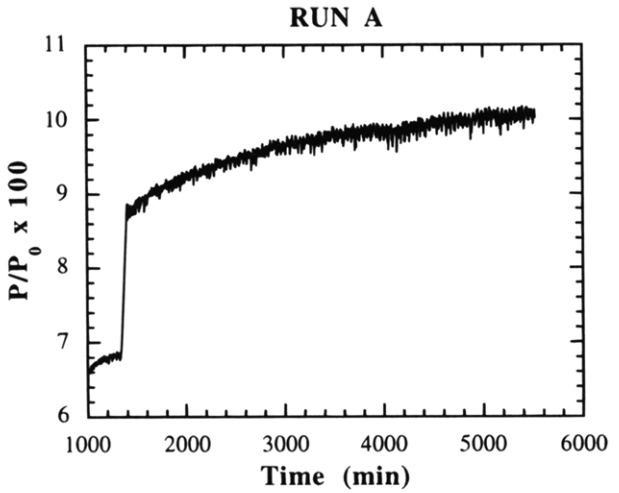

Figure 4. Tempering trajectory for run A. Linear plot, times > 1000 min.

about 5 h before the second quench. Our expectation that longer tempering times lead to larger grain sizes is consistent with our experimental data. In Figure 3, the tempering trajectory of run A is plotted as a function of time. We can roughly divide the curve into three regions represented by 1−3. For the first 300 min after the sample was quenched from the disordered state, the birefringence did not change at all; thus, in region 1, the grains (if they exist) are too small or weak to be detected with light. As time proceeded, the birefringence started to develop, and the growth rate was increasing. The rate $[d(P/P_0)/dt]$ reached a maximum of 1.4×10^{-4} min^{-1}, after which it slowed down and eventually leveled off. Evidently, region 2 is the principal region of grain growth. In region 3, the birefringence still increased with time, and the rate was calculated to be 2.5×10^{-6} min^{-1}.

Quenching the sample to 22 °C caused a jump in birefringence that is qualitatively similar to previous measurements[5] and is due to the temperature dependence of $\Delta n = n_e - n_o$, where n_e and n_o are the extraordinary and ordinary refractive indices. The birefringence at this stage is plotted as a function of time in Figure 4. The birefringence at 22 °C clearly continues to increase with time, and the rate was calculated to be 2.8×10^{-6} min^{-1}, which is approximately the same as the rate in region 3 of Figure 3 before the final quench. It is somewhat surprising that grains can grow at 22 °C. At this temperature, the polystyrene-rich cylindrical phase is 19 °C below its glass transition temperature. Such growth was not observed in lamellar SI block copolymers below the T_g of the polystyrene-rich phase. It is thus evident that the mobility of the polyisoprene matrix is mainly responsible for grain growth in the cylindrical sample. However, the final stages of annealing imperfections requires some mobility in the polystyrene-rich phase.

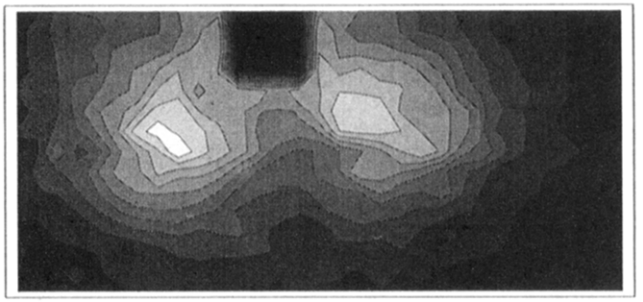

Figure 5. Experimental H_V scattering pattern from diblock copolymer SI(4-13), run B. Two quadrants are shown. Full vertical scale is 0.0583 rad. A central bright spot, due to leakage of the incident beam through the analyzer, has been blacked out. The beam center is located at the top edge of the plot, at the center of the blacked-out region.

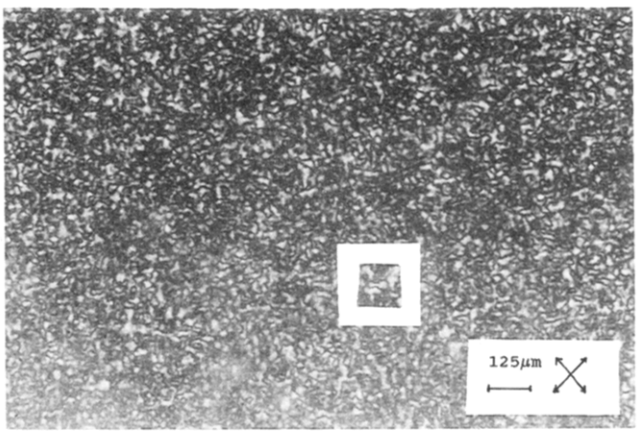

Figure 6. Polarized light micrograph of thin diblock copolymer sample. Scale and orientation of the polarizers are indicated. A box has been drawn around one of the grain pairs.

All samples studied exhibited a 4-fold cloverleaf H_V scattering pattern with an off-axis maximum. The two-dimensional scattering pattern obtained from the ordered sample B described above is shown in Figure 5. The qualitative features are independent of tempering time, although the angular spread decreases with tempering time. This is consistent with the growth of larger grains for longer tempering times.

C. Polarized-Light Microscopy. Optical microscopy was performed with a Nikon Optiphot polarized-light microscope. Samples were prepared by squeezing the polymer between a glass microscope slide and a cover slip. Such samples, with thicknesses of approximately several tenths of a millimeter, were heated above T_{ODT}, followed by tempering at 53.5 °C and quenching to 22 °C. Depolarized light scattering from such samples exhibited the same cloverleaf pattern reported in Figure 5. Microscopy revealed the fairly detailed structure of single layers of grains, as shown in Figure 6. The field of the microscope was divided into micron-dimensioned regions of low and high intensity; we associate the bright regions with grains whose optic axes are at ±45° to the polarizer axis. The bright regions tend to be oblong shaped with shape axes also

at ±45° to the polarizer axis. The other evident feature is the propensity of closely-spaced pairs of bright regions, separated by a narrow dark region.

By interposing a quartz quarter-wave retardation plate between the polarizers, one can distinguish between grains with optic axes at +45° and −45° to the polarizer axis. Rotating the quarter-wave plate in one direction will tend to cancel the retardation, and thus decrease the intensity, of one grain type, while rotating in the other direction tends to cancel the retardation of the other. Furthermore, because the dispersion of the retardation of the quartz does not match the dispersion of the retardation of the polymer, different wavelength components of the transmitted white light will be better or worse compensated, giving rise to a reddish tint for one type of grain and a bluish tint to the other.[12] With a quarter-wave plate whose optic axis is tilted less than 1° away from the polarizer axis, we observe that paired grains tend to have one member tinted blue and the other red, suggesting that their optic axes are at right angles to each other.

One possible interpretation of the dark line separating a pair of grains is that the optic axis is continuously changing from one region to the other and is exactly parallel (or perpendicular) to the polarizer at the dark line. This can be tested by observing a field of the sample while rotating the polarizer and analyzer together. The dark line should continuously move toward one region or the other depending on the direction of rotation. We observe that these dark lines do not move while rotating the polarizers. Instead, the bright regions alternately brighten and darken as the polarizers are rotated. We therefore conclude that the optic axes are approximately constant within each grain and interpret the dark line as the diffraction-limited boundary between the grain pair, where the superposition of overlapping diffracted light from each other grain is interfering destructively.

While rotating both polarizer and analyzer, one can occasionally observe the continuous movement of a bright feature from one location to another. This is evidence of a continuously changing optic axis, although this behavior is unusual for SI(4-13). The most common behavior is for regions to brighten or darken uniformly as the polarizer/analyzer pair is rotated. This is evidence for a grain structure in which the optic axis is constant and between which there is a discontinuous change in optic axis.

We emphasize that our microscopy results on cylindrical block copolymers are quite different from those obtained from thin films of liquid crystalline polymers or from spherulitic samples. In liquid crystals, one observes dark lines rotating continuously about disclination axes as polarizer and analyzer are rotated.[13] In spherulitic polymers, one sees Maltese cross patterns which rotate as the polarizer and analyzer are rotated.[14] We do not see either of these signatures and thus conclude that the structural origin of the cloverleaf pattern in cylindrical block copolymers must be quite different and related to the presence of correlated grain pairs.

III. Theoretical Models

A. Background. Four-fold cloverleaf H_V scattering patterns have been observed in many systems consisting of anisotropic structural elements, including spherulites, anisotropic rodlike or disklike crystallites, and nematic liquid crystals. In some cases, the lobes are parallel to the polarizer and analyzer axes (+ type), and in others, they make an angle of 45° (× type). In some cases, the scattering intensity is a maximum in the forward direction, and in others, the maximum occurs at some angle away from the forward direction. Various models have been developed to account for the scattering in specific cases, including anisotropic spheres with different radial and tangential polarizabilities,[8] randomly oriented anisotropic rods or disks with a definite angle between the shape axis and optic axis,[15,16] and a continuously varying director with complex geometry in the vicinity of the disclination axes.[10,17]

Most of these models involve scattering elements of a specific size and employ a mathematical procedure called the amplitude method.[18] In this method, a specific geometrical model of the anisotropic elements is used to calculate the scattered field, and the intensity is found by averaging the absolute square of the far-field distribution over a random arrangement of element orientations. We have considerable microscopic evidence that the grain structure of block copolymers involves not only random orientations but also random shapes and sizes of grains. Because the amplitude method requires a specific grain geometry, it cannot realistically represent the actual structure of a block copolymer sample. We have therefore employed an alternative mathematical procedure termed the correlation function method,[18] in which the expression for the square of the field is represented as a double integral involving products of grain shape functions. Averages performed at this stage lead to a description of the far-field intensity in terms of correlations of the grain shape functions.

In most earlier applications of the correlation function method, the correlation function was assumed to be spherically symmetric, giving rise to an azimuthally symmetric scattering pattern. The restrictive nature of this assumption was commented on by both Stein and van Aartsen.[19,20] Several earlier attempts to allow the correlation function to decay at different rates in different directions gave results that were unwieldy and not easily applied.[20,21] In this paper, we have developed a model that overcomes these problems. We assume that the optic axis is fixed in orientation within a grain. Our ensemble averaging is done in two steps. First we consider all grains whose shape axes have a particular orientation. We average over the shapes of those grains. This does not involve the optic axis orientations. Then we average over all possible grain orientations. Our model allows for the separability of these two stages of averaging.

Robust experimental features of the far-field scattering from the cylindrical block copolymers we have studied are (1) a 4-fold, ×-type scattering pattern and (2) an off-axis maximum; an adequate model ought to exhibit both features. One potential candidate that is consistent with the rectilinear textures seen in microscopy is an anisotropic rod model. If either the amplitude or correlation function method is applied to randomly oriented anisotropic rods with an optic axis at a fixed angle with respect to the rod axis, one obtains a 4-fold scattering pattern [ref 15 and section III.F.1 of this paper]. If the angle is 0°, one gets ×-type scattering, whereas if the angle is 45°, the pattern is of the + type. Other angles will lead to either a + or ×-type pattern, but in all cases, the greatest scattered intensity is directed on-axis, and the off-axis distributions decay monotonically from the forward direction. Since our

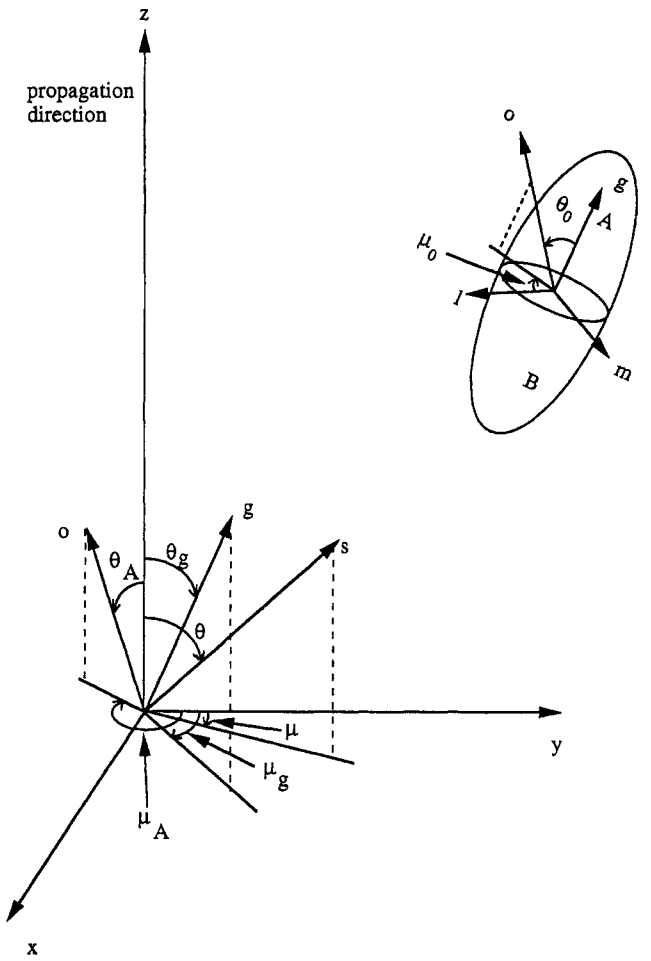

Figure 7. Schematic of CGP geometry. The vectors **o** and **g** are each shown twice: once in the laboratory frame and once in the CGP frame. The ellipsoidal shape used is merely a schematic representation of a CGP. Actual CGPs are highly irregular in shape and have a distribution of sizes.

observed patterns consistently possess off-axis maxima, they are incompatible with the anisotropic rod model.

Any model that involves uncorrelated grains with constant optic axes will exhibit an intensity maximum in the forward direction, since radiation from each volume element of a grain interferes constructively in the forward direction. If the optic axis were allowed to vary in direction within the volume of coherent order, then suppression of the forward scattering is possible, leading to the development of off-axis maxima. A simple model that incorporates a varying optic axis, and one that is suggested by our observations by microscopy, consists of a random collection of correlated grain pairs, with a constant optic axis within each grain of the pair.

B. Formulation. We will assume that in a statistical sense (to be explained below), the correlated grain pairs (CGPs) can be characterized as consisting of two regions, which we call grains, designated A and B, aligned along a CGP axis. In each grain the optic axis points in a different, but fixed, direction relative to the CGP axis. Figure 7 is descriptive of such a CGP. We assume that the incident x-polarized beam propagates in the z direction. We denote the polar and azimuthal angular coordinates of each grain's optic axis, referred to the x, y, z laboratory coordinates, as $\{\theta_A, \mu_A\}$ and $\{\theta_B, \mu_B\}$, respectively. The unsubscripted variables θ and μ are the polar and azimuthal angles of the unit vector **s** directed from the sample toward the far-field point $\mathbf{r}_{ff}$. All these polar angles are measured from the z axis, and azimuthal angles from the $z-y$ plane. The angular coordinates of the optic axes, referred to an orthogonal coordinate system $\{g, l, m\}$ using the CGP's axis, **g**, as the polar axis, are $\{\theta_{0A}, \mu_{0A}\}$ and $\{\theta_{0B}, \mu_{0B}\}$, respectively. The **l** axis is chosen to be normal to the $g-z$ plane, and the azimuthal angles are measured from the $g-l$ plane.

Application of the Rayleigh approximation[22] to our configuration gives the H_V electric field component radiated by the ith CGP, at the far-field point $\mathbf{r}_{ff}$:

$$E_i = \frac{C}{r_{ff}} e^{-ik\mathbf{a}_z\cdot\mathbf{r}_{ff}} \int d\mathbf{r}' \{\sin^2(\theta_A)\sin(2\mu_A) f_{A_i}(\mathbf{r}') e^{i\kappa\cdot(\mathbf{r}_{ff}-\mathbf{r}')} + \sin^2(\theta_B)\sin(2\mu_B) f_{B_i}(\mathbf{r}') e^{i\kappa\cdot(\mathbf{r}_{ff}-\mathbf{r}')}\} \quad (1)$$

where

$$C = \frac{E_0 k^2 n(n_e - n_o)}{2\pi}$$

$$\kappa = k(\mathbf{s} - \mathbf{a}_z) = k(\mathbf{a}_z(\cos\theta - 1) + \mathbf{a}_x \sin\theta \sin\mu + \mathbf{a}_y \sin\theta \cos\mu)$$

$$\mathbf{r}_{ff} = r_{ff}(\mathbf{a}_z \cos\theta + \mathbf{a}_x \sin\theta \sin\mu + \mathbf{a}_y \sin\theta \cos\mu) \quad (2)$$

In eq 1 $f_{A_i}(\mathbf{r})$ and $f_{B_i}(\mathbf{r})$ are the shape functions for the A and B grains of the ith CGP, equal to unity when the position vector **r** is in the corresponding grain and 0 otherwise, and $\mathbf{a}_x$, $\mathbf{a}_y$, $\mathbf{a}_z$ are unit vectors in the x, y, z directions, respectively. E_0 is the incident field amplitude, n is the average refractive index, and $k = n\omega/c$.

If the wavelength in the medium is much less than the smallest linear dimension of the CGP, we may use the *paraxial approximation*:

$$\kappa \approx k(\mathbf{a}_x \sin\theta \sin\mu + \mathbf{a}_y \sin\theta \cos\mu) \quad (3)$$

Since we have a random arrangement of uncorrelated CGPs, we average over a representative ensemble of the sample. The angular brightness (intensity per unit solid angle) is given by

$$\frac{dI}{d\Omega} = \underset{\text{orientation angles}}{\text{av over CGP}} C^2 \int\int d\mathbf{r}'\, d\mathbf{r}''\, e^{i\kappa\cdot(\mathbf{r}'-\mathbf{r}'')} \times \{\sin^4(\theta_A)\sin^2(2\mu_A)\sum_i \langle f_{A_i}(\mathbf{r}') f_{A_i}(\mathbf{r}'')\rangle + \sin^4(\theta_B)\sin^2(2\mu_B)\sum_i \langle f_{B_i}(\mathbf{r}') f_{B_i}(\mathbf{r}'')\rangle + \sin^2(\theta_A)\sin^2(\theta_B)\sin(2\mu_A)\sin(2\mu_B) \times \sum_i [\langle f_{A_i}(\mathbf{r}') f_{B_i}(\mathbf{r}'')\rangle + \langle f_{B_i}(\mathbf{r}') f_{A_i}(\mathbf{r}'')\rangle]\} \quad (4)$$

The position vectors $\mathbf{r}'$ and $\mathbf{r}''$ refer to two points in the sample that make contributions to the far-field scattering pattern at the point $\mathbf{r}_{ff}$. The angle brackets represent ensemble averages over CGPs of a particular CGP axis orientation. The i sums are probabilities whose meanings follow from the following considerations. For each realization of the ensemble, the product $f_{A_i}(\mathbf{r}')$ $f_{A_i}(\mathbf{r}'')$ is 1 if both $\mathbf{r}'$ and $\mathbf{r}''$ are in the A grain of the ith CGP; otherwise it is 0. Thus, the probabilities, P_A and P_B, that both points are in the same A or same B grain of some CGP are

$$P_A = \sum_i \langle f_{A_i}(\mathbf{r}')\, f_{A_i}(\mathbf{r}'')\rangle \qquad P_B = \sum_i \langle f_{B_i}(\mathbf{r}')\, f_{B_i}(\mathbf{r}'')\rangle \quad (5)$$

The sum of the two probability functions starts at unity when $\mathbf{r}' = \mathbf{r}''$ and decreases toward zero when the distance between the two points, along any direction, increases past the average grain size in that direction. The probability that $\mathbf{r}'$ and $\mathbf{r}''$ are in different grains of the same CGP is

$$P_{\text{diff grains}}^{\text{same CGP}} = \sum_i [\langle f_{A_i}(\mathbf{r}')\, f_{B_i}(\mathbf{r}'')\rangle + \langle f_{B_i}(\mathbf{r}')\, f_{A_i}(\mathbf{r}'')\rangle] \quad (6)$$

Equations 5 and 6 give physical meaning to the factors which appear in the expression for the angular brightness, eq 4. We will assume forms for these factors consistent with our statistical model. The reasoning that leads to assumed forms for eq 5, where both points are in the same grain, is more direct than for eq 6, where each point is in a different grain. However, we can relate the probability that each point is in a different grain, to the probability that both points are in the same CGP and that both points are in the same grain. The probability that both points are in the same CGP is

$$P_{\text{same CGP}} = \sum_i \langle (f_{A_i}(\mathbf{r}') + f_{B_i}(\mathbf{r}'))(f_{A_i}(\mathbf{r}'') + f_{B_i}(\mathbf{r}''))\rangle \quad (7)$$

On expanding (7), we get the obvious relation

$$P_{\text{same CGP}} = P_{\text{same grain}} + P_{\text{diff grain}}^{\text{same CGP}} \quad (8)$$

where $P_{\text{same grain}} = P_A + P_B$.

C. Considerations Which Restrict the Assumed Form of the Correlation Functions. In our context, the probability functions discussed above are two-point correlation functions. In the correlation function approach to scattering problems, a physical model of the scatterers is used to motivate assumptions concerning the mathematical form of the correlation functions. A difficulty with this procedure is that apparently reasonable assumed forms can lead to nonphysical intensity distributions. An example of such a nonphysical output would be a negative value for the calculated scattered intensity over some range of angles. A more subtle case can occur in our problem when the calculated intensity pattern is inconsistent with the statistical dispersion of the geometrical parameters of the grains within a CGP. Restrictions on the possible assumed forms of the correlation functions are implied by the following considerations:

From eqs 5–8 we have

$$\sum_i \langle (\int d\mathbf{r}'[f_{A_i}(\mathbf{r}') - f_{B_i}(\mathbf{r}')])^2\rangle = N\langle (V_A - V_B)^2\rangle =$$

$$\int\int d\mathbf{r}'\, d\mathbf{r}''\, [2P_{\text{same grain}}^{\text{same CGP}}(\mathbf{r}',\mathbf{r}'') - P_{\text{same CGP}}(\mathbf{r}',\mathbf{r}'')] \quad (9)$$

where N is the number of illuminated CGPs in the sample with a particular CGP axis orientation, and V_A and V_B are volumes of grains A and B, respectively. We also have

$$\int\int d\mathbf{r}'\, d\mathbf{r}''\, P_{\text{same grain}}(\mathbf{r}',\mathbf{r}'') = N\langle {V_A}^2 + {V_B}^2\rangle$$

$$\int\int d\mathbf{r}'\, d\mathbf{r}''\, P_{\text{same CGP}}(\mathbf{r}',\mathbf{r}'') = N\langle {V_{CGP}}^2\rangle \quad (10)$$

We define the relative difference in grain volumes squared as

$$\Delta \equiv \frac{\langle (V_A - V_B)^2\rangle}{\langle V_A\rangle^2 + \langle V_B\rangle^2} \quad (11)$$

The quantity Δ ranges from 0, when each of the two grains of each CGP have the same volume, to 1, when the volume of one grain is zero. Any assumed form of correlation function will implicitly presuppose a particular spread to the distribution of grain volumes. When there is no statistical distinction between the grains we get, from eqs 10 and 11

$$\Delta = 2 - \frac{\langle {V_{CGP}}^2\rangle}{2\langle {V_{grain}}^2\rangle} \quad (12)$$

D. Statistical Model of CGPs. In an earlier paper,[6] we defined a spherically symmetric Gaussian correlation function with a single size parameter, w, to model grains that were, on average, spherically symmetric. We now wish to model grains and CGPs that are, on average, ellipsoids of revolution. We emphasize, however, that actual CGPs are highly irregular in shape and have a distribution of sizes. Thus we require a correlation function that is characterized by two size parameters (ℓ, w) depending on the direction relative to the CGP axis. We define the correlation functions

$$C_{A,A}(\mathbf{r}'-\mathbf{r}'') = \frac{1}{2}\exp\left[-\left(\frac{\mathbf{g}\cdot(\mathbf{r}'-\mathbf{r}'')}{\ell f}\right)^2\right] \times \exp\left[-\frac{(\mathbf{l}\cdot(\mathbf{r}'-\mathbf{r}''))^2 + (\mathbf{m}\cdot(\mathbf{r}'-\mathbf{r}''))^2}{w^2}\right]$$

$$C_{A+B,A+B}(\mathbf{r}'-\mathbf{r}'') = \exp\left[-\left(\frac{\mathbf{g}\cdot(\mathbf{r}'-\mathbf{r}'')}{\ell}\right)^2\right] \times \exp\left[-\frac{(\mathbf{l}\cdot(\mathbf{r}'-\mathbf{r}''))^2 + (\mathbf{m}\cdot(\mathbf{r}'-\mathbf{r}''))^2}{w^2}\right] \quad (13)$$

where $\mathbf{g}$ is a unit vector in the direction of the CGP axis and $\{\mathbf{g}, \mathbf{l}, \mathbf{m}\}$ constitute an orthogonal set of unit vectors. We make the assumptions

$$P_{\text{same grain}} = 2C_{A,A}(\mathbf{r}'-\mathbf{r}'')$$

$$P_{\text{same CGP}} = C_{A+B,A+B}(\mathbf{r}'-\mathbf{r}'') \quad (14)$$

The factor, f, which enters in eq 13, is determined by the statistical spread in grain lengths. From eqs 9–13 we get

$$f = \frac{1}{2-\Delta} = \frac{2\langle {V_{grain}}^2\rangle}{\langle {V_{CGP}}^2\rangle} \quad (15)$$

E. Evaluation of the Scattering Patterns. By relating the shape functions in eq 4 to probabilities (eqs 5–8), and those probabilities to correlation functions (eqs 13 and 14), we can show that the H_V intensity for the CGP orientation in the differential solid angle centered at $\{\theta_g, \mu_g\}$ is proportional to

$$(F^2(\theta_g,\mu_g,\theta_{0_A},\mu_{0_A}) + F^2(\theta_g,\mu_g,\theta_{0_B},\mu_{0_B})) \times \int\int d\mathbf{r}'\, d\mathbf{r}''\, C_{AA}(\mathbf{r}'-\mathbf{r}'')\, e^{i\kappa(\mathbf{r}'-\mathbf{r}'')} + F(\theta_g,\mu_g,\theta_{0_A},\mu_{0_A})\, F(\theta_g,\mu_g,\theta_{0_B},\mu_{0_B}) \times \int\int d\mathbf{r}'\, d\mathbf{r}''\, (C_{A+B,A+B}(\mathbf{r}'-\mathbf{r}'') - 2C_{A,A}(\mathbf{r}'-\mathbf{r}''))\, e^{i(\kappa(\mathbf{r}'-\mathbf{r}''))} \quad (16)$$

where

$$F(\theta_g,\mu_g,\theta_{0_\alpha},\mu_{0_\alpha}) = \sin^2(\theta_\alpha)\sin(2\mu_\alpha) \quad (17)$$

and the α subscript stands for A or B (see Appendix A). In order to facilitate the evaluation of the spatial integrals, we represent $\mathbf{r}' - \mathbf{r}''$ in the $\{\mathbf{g}, \mathbf{l}, \mathbf{m}\}$ system and use

$$\kappa\cdot\mathbf{g} \approx \frac{2\pi}{\lambda}\theta\sin(\theta_g)\cos(\mu-\mu_g) \quad (18)$$

Integrating over $\mathbf{r}'$ and $\mathbf{r}''$ and averaging over CGP orientations, the resultant expression for the angular brightness is given by

$$\frac{dI}{d\Omega} = C^2\int_0^\pi d\theta_g\, P_\theta(\theta_g)\sin\theta_g\int_0^{2\pi}d\mu_g\int_0^{2\pi}d\mu_0\, P_\mu(\mu_0) \times \{(F_A{}^2(\theta_g,\mu_g,\theta_{0_A},\mu_0) + F_B{}^2(\theta_g,\mu_g,\theta_{0_B},\mu_0+\Delta\mu)) \times fK(\theta_N,\theta_g,\mu-\mu_g;\ell/f) + 2F_A(\theta_g,\mu_g,\theta_{0_A},\mu_0)\, F_B(\theta_g,\mu_g,\theta_{0_B},\mu_0+\Delta\mu) \times [K(\theta_N,\theta_g,\mu-\mu_g;\ell) - fK(\theta_N,\theta_g,\mu-\mu_g;\ell/f)]\} \quad (19)$$

where

$$K(\theta_N,\theta_g,\mu-\mu_g;\ell) = Ne^{-\theta_N{}^2}e^{-\theta_N{}^2((\ell/w)^2-1)\sin^2\theta_g\cos^2(\mu-\mu_g)} \quad (20)$$

and where $\theta_N = kw\theta/2$. The coefficients P_θ and P_μ are probability densities, $\mu_0 = \mu_{0A}$, and $\Delta\mu$ is the difference in the azimuthal angle of the optic axes in the two grains.

It follows from the form of the F coefficients given in eq A3 that $F_\alpha F_\beta(\mu_g + \pi/2) = F_\alpha F_\beta(\mu_g)$ and is therefore 4-fold symmetric in μ_g. Furthermore, the integrals over μ_0 are expressions linear in $\cos(4\mu_g)$ and are of the form

$$\int_0^{2\pi}d\mu_0\, P_\mu(\mu_0)\, F_\alpha F_\beta = a_{\alpha,\beta}(\theta_g) + b_{\alpha,\beta}(\theta_g)\cos(4\mu_g) \quad (21)$$

It will be seen from the following arguments leading to eq 26 that this form implies a radiation pattern with an even, 4-fold symmetry in μ. From the expansion

$$e^{-z\cos\phi} = \sum_{m=0}^{\infty}\epsilon_m(-1)^m I_m(z)\cos(m\phi) \quad (22)$$

where I_m is the modified Bessel function and

$$\epsilon_m = \begin{cases}1 & m=0\\ 2 & m>0\end{cases} \quad (23)$$

we get

$$K(\theta_N,\theta_g,\mu-\mu_g;\ell) = Ne^{-\theta_N{}^2}e^{-(1/2)\theta_N{}^2((\ell/w)^2-1)\sin^2\theta_g} \times \sum_{m=0}^{\infty}\epsilon_m(-1)^m I_m\left(\frac{1}{2}\theta_N{}^2\left(\left(\frac{\ell}{w}\right)^2-1\right)\sin^2\theta_g\right) \times \cos(2m(\mu-\mu_g)) \quad (24)$$

and

$$\frac{dI}{d\Omega} = C^2\int_0^\pi d\theta_g\sin\theta_g\, P_\theta(\theta_g)\int_0^{2\pi}d\mu_g\,(a_{AA}(\theta_g) + a_{BB}(\theta_g) - 2a_{AB}(\theta_g))fK(\theta_N,\theta_g,\mu-\mu_g;\ell/f) + 2a_{AB}(\theta_g)\,K(\theta_N,\theta_g,\mu-\mu_g;\ell) + (b_{AA}(\theta_g) + b_{BB}(\theta_g) - 2b_{AB}(\theta_g))\cos(4\mu_g)\,fK(\theta_N,\theta_g,\mu-\mu_g;\ell/f) + 2b_{AB}(\theta_g)\cos(4\mu_g)\,K(\theta_N,\theta_g,\mu-\mu_g;\ell) \quad (25)$$

The μ_g integral leads to cancelation of the contributions from all terms in the expansion of K, in eq 25, except for two. The expression for angular brightness has the form

$$\frac{dI}{d\Omega} = C(\theta_N) + D(\theta_N)\cos(4\mu) \quad (26)$$

where

$$C(\theta_N) = 2\pi fe^{-\theta_N{}^2}\int_0^\pi d\theta_g\sin\theta_g\, P(\theta_g)\, e^{-\beta(\ell/f,\theta_g)} \times (a_{AA}(\theta_g) + a_{BB}(\theta_g) - 2a_{AB}(\theta_g))I_0(\beta(\ell/f,\theta_g)) + 4\pi e^{-\theta_N{}^2}\int_0^\pi d\theta_g\, P(\theta_g)\sin\theta_g\, e^{-\beta(\ell,\theta_g)}a_{AB}(\theta_g)\, I_0(\beta(\ell,\theta_g)) \quad (27)$$

and

$$D(\theta_N) = 2\pi fe^{-\theta_N{}^2}\int_0^\pi d\theta_g\sin\theta_g\, P(\theta_g)\, e^{-\beta(\ell/f,\theta_g)} \times (b_{AA}(\theta_g) + b_{BB}(\theta_g) - 2b_{AB}(\theta_g))I_2(\beta(\ell/f,\theta_g)) + 4\pi e^{-\theta_N{}^2}\int_0^\pi d\theta_g\, e^{-\beta(\ell,\theta_g)}\sin\theta_g\, P(\theta_g)\, b_{AB}(\theta_g)\, I_2(\beta(\ell,\theta_g)) \quad (28)$$

The argument β is given by

$$\beta(\ell,\theta_g) = \frac{1}{2}\theta_N{}^2\left(\left(\frac{\ell}{w}\right)^2-1\right)\sin^2\theta_g \quad (29)$$

The method used to determine the a and b coefficients and their values for several model geometries are described in Appendix A.

F. Results of Model Calculations. Case 1. One Grain per CGP, Full 3D Averaging. The two-grain CGP model reduces to a one-grain model when $\theta_{0A} = \theta_{0B}$ and $\mu_{0A} = \mu_{0B}$. When $\theta_{0A} = 0$, it describes a rod model with the optic axis parallel to the rod axis. Figure 8a displays the scattered intensities as a function of θ, along two azimuthal directions $\mu = 0$ and $\pi/4$, for various values of the ratio of the characteristic rod length to diameter, ℓ/w. In all cases, the intensity maximum is in the forward direction. For $\ell = w$, the grains are on average spheres, and the pattern shape reduces to one with azimuthal symmetry. For $\ell/w = 4$ and $1/4$, the average grains are similar to prolate and oblate ellipsoids of revolution, respectively. In both cases, the pattern has a 4-fold symmetry with lobes at ±45° to the polarizer and analyzer axes. Figure 8b shows a contour plot of the calculated scattered intensity for $\ell/w = 4$.

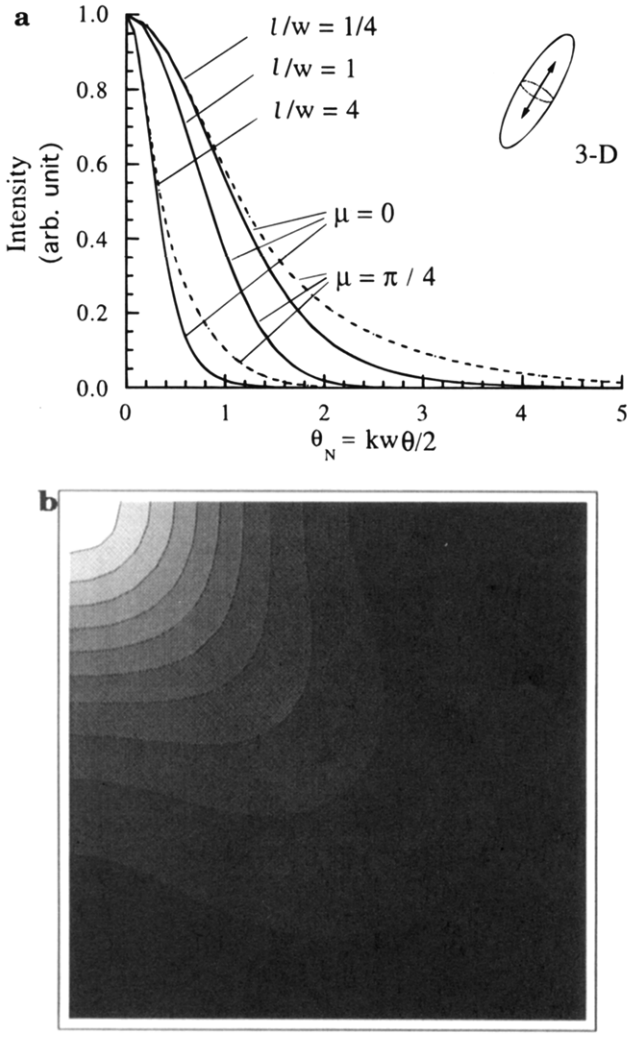

Figure 8. (a) Scattered intensity as a function of reduced scattering angle. Solid line for azimuthal angle $\mu = 0$; dotted line for $\mu = 45°$. Case 1: Ellipsoidal grains with optic axis parallel to grain axis. l = characteristic dimension of grain along grain axis; w = characteristic dimension of grain along axis perpendicular to grain axis. The values of l/w used for each of the cases 1–6 were chosen to show the range of behavior in that case. Diagram to right of graph shows schematic representation of grain geometry. (b) Contour plot for $l/w = 4$. Full horizontal scale is $\theta_N = 5$. One quadrant is shown. The incident beam is located in the upper left corner.

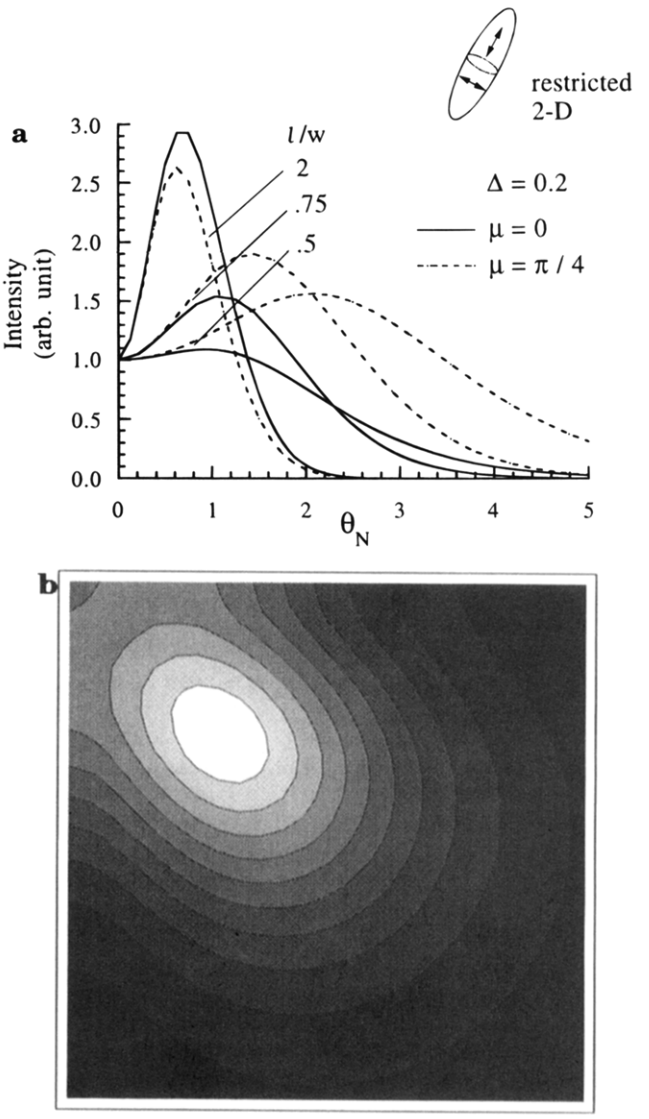

Figure 9. (a) Case 2: Scattered intensity. Two grains per CGP, restricted 2D problem (CGP axis and optic axis confined to plane perpendicular to direction of incident beam). (b) Contour plot for $l/w = 0.75$. Full horizontal scale is $\theta_N = 5$. The incident beam is located in the upper left corner.

Case 2. Two Grains per CGP, Restricted 2D Problem. In this case, the CGP shape axis is restricted to be perpendicular to the incident beam. The two optic axes are also restricted to be perpendicular to the incident beam. Figure 9 illustrates the special case of $\theta_{0A} = 0$ and $\theta_{0B} = \pi/2$; i.e. the optic axis of one grain is parallel to the CGP shape axis, and the other is perpendicular. In cases 2–6, l and w refer to CGP dimensions, whereas f and w refer to individual grain dimensions. The value $\Delta = 0.2$ has been used in the model calculations, making $f = 0.56$. For $l/w = 2$, one sees a +-type scattering pattern [$dI/d\Omega(\mu=0) > dI/d\Omega(\mu=\pi/4)$], while for $l/w = 0.75$ and 0.5, the pattern is of the × type [$dI/d\Omega(\mu=0) < dI/d\Omega(\mu=\pi/4)$]. In all cases there is a significant reduction of the intensity in the forward direction, as expected.

Case 3. Two Grains per CGP, Unrestricted 2D Problem. This case is similar to the previous one, except that the optic axes are not restricted to the plane perpendicular to the incident beam. For the special case $\theta_{0A} = 0$ and $\theta_{0B} = \pi/2$, Figure 10 shows that the contrast of the lobes is reduced, and in one case ($l/w = 0.5$), the off-axis maximum is lost.

Case 4. Two Grains per CGP, $\theta_{0A} = 0$, $\theta_{0B} = \pi/2$, Full 3D Averaging. This case is similar to both cases 2 and 3 except that full three-dimensional averaging is performed for the special case that one grain has an optic axis parallel to the CGP axis and the other is perpendicular. Figure 11 shows that, for $l/w = 1$ and 0.25, the off-axis maximum is lost, while for $l/w = 4$, the pattern is of the + type.

Case 5. Two Grains per CGP, $\theta_{0A} = \theta_{0B} = \pi/2$, $\mu_{0A} = \mu_{0B} + \pi/2$, Full 3D Averaging. In this case, both grains have optic axes perpendicular to the CGP axis, but perpendicular to each other. The off-axis maximum is lost for $l/w = 1$ and $1/8$, while a weak × pattern with off-axis maximum is obtained for $l/w = 8$ (see Figure 12).

Case 6. Two Grains per CGP, $\theta_{0A} = \pi/4$, $\theta_{0B} = 3\pi/4$, $\mu_{0A} = \mu_{0B}$, Full 3D Averaging. Here, one grain has an optic axis at +45° to the CGP axis and the other grain has an optic axis at −45°. For $l/w = 4$, a fairly strong × pattern is obtained, with a definite off-axis maximum (Figure 13).

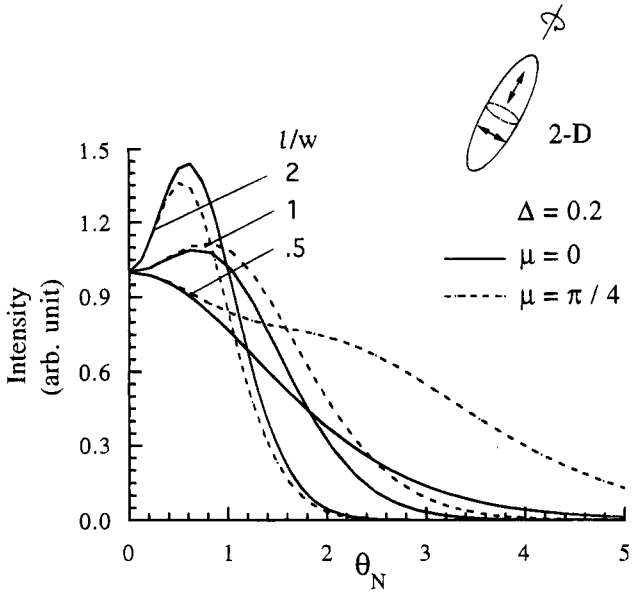

Figure 10. Case 3: Scattered intensity. Two grains per CGP, unrestricted 2D problem (only CGP axis confined to plane perpendicular to direction of incident beam).

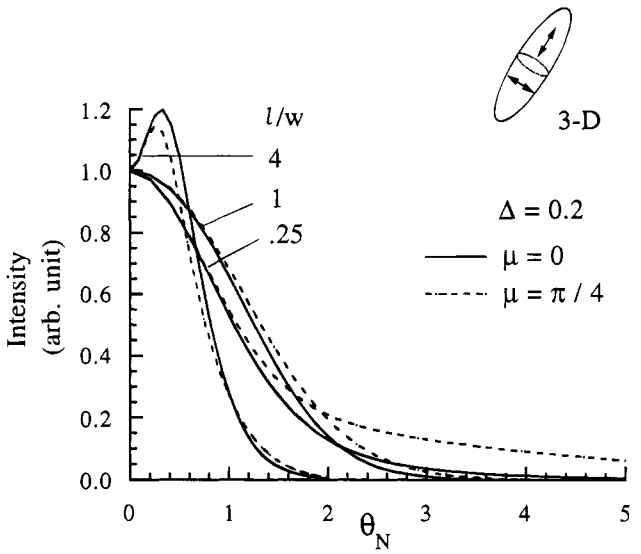

Figure 11. Case 4: Scattered intensity. Two grains per CGP, full 3D averaging. One optic axis parallel and one optic axis perpendicular to CGP axis.

Of all the cases examined, case 2 leads to a radiation pattern that best matches our experimental results. In this model, the optic and shape axes of the CGPs are restricted to lie in the plane perpendicular to the incident beam. Of course our actual grains are three-dimensional, so a 2D model would apply only if the dimension of a grain pair, in the direction perpendicular to the plane containing the two optic axes, is much longer than ℓ or w. In such a case, the primary contributors to the far-field pattern are those pairs whose longest dimension is parallel to the direction of propagation, and the 2D model represents a good approximation. It is possible to extend the model to include grains and CGPs with three distinct dimensions (ℓ, w_1, w_2) although the increased computational complexity is substantial.

The scattering maximum can be related to the average grain dimensions. In all cases, the peak intensity for an ×-type pattern falls between $\theta_N = 0.5$ and 2. Taking the best case as case 2 with $\ell/w = 0.75$, we get

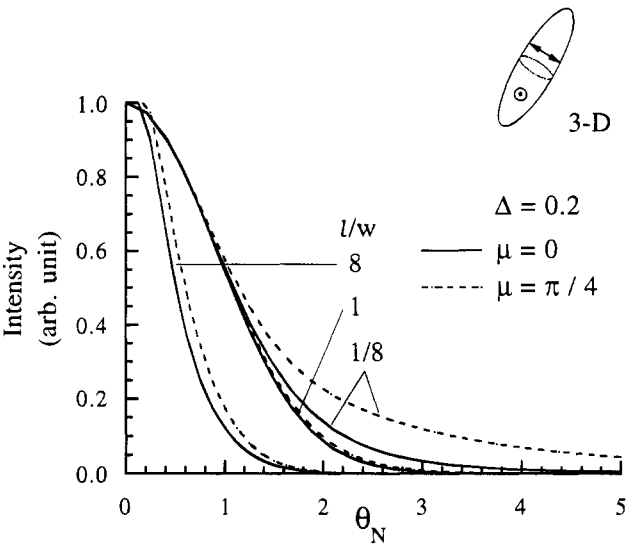

Figure 12. Case 5: Scattered intensity. Two grains per CGP, full 3D averaging. Both optic axes perpendicular to CGP axis and perpendicular to each other.

$\theta_N = 1.5$ at peak intensity. Relating this to the experimental profile shown in Figure 5, where the peak falls at $\theta_{max} = 0.031$ rad, we calculate $\ell = 7.4$ μm and $w = 10$ μm [$w = 1.5\lambda/\pi\theta_{max}$]. This is in reasonable qualitative agreement with grain dimensions inferred from micrographs (e.g. Figure 6). Quantitative interpretation of micrographs would require numerous assumptions. In addition, the exact geometry and thermal history of samples shown in Figures 5 and 6 are not identical.

IV. Discussion and Concluding Remarks

Light scattering patterns from quiescently-ordered, cylindrical-morphology diblock-copolymer melts showed a surprising 4-fold symmetry with lobes where μ is an odd multiple of 45° and with off-axis maxima. This indicates the presence of orientation correlations on the micron length scale. This was corroborated by the observation of correlated grain pairs by polarized light microscopy. The correlated-grain-pair model was developed to describe the nature of these correlations. We have shown that the small-angle light scattering pattern can be simply described by $dI/d\Omega = C(\theta_N) + D(\theta_N)\cos(4\mu)$, where the functions C and D depend on the shape, size, and relative optic axis orientation of the correlated grains.

We have developed theoretical methods that are effective for the analysis of correlated grain pairs. Although the ×-type scattering pattern with off-axis maximum is a robust feature of the experimental data, it is observed in the CGP model only for a very limited subset of parameters. Of the limited cases studied, the best qualitative match between theory and experiment is obtained in case 2 (restricted 2D case). Given the limited region of parameter space studied, it is premature to judge the ultimate success or failure of the CGP model. Further experimental evidence from electron microscopy could aid in suggesting on what regions of parameter space to focus attention. Alternatively, the CGP model may be insufficient to quantitatively describe the structure of block copolymer grains. Even if this proves true, the theoretical methods that have been devised to study this model have pertinence to other compound structures. Thus, we believe that these methods represent an important first step in the understanding of the correlations that arise spontane-

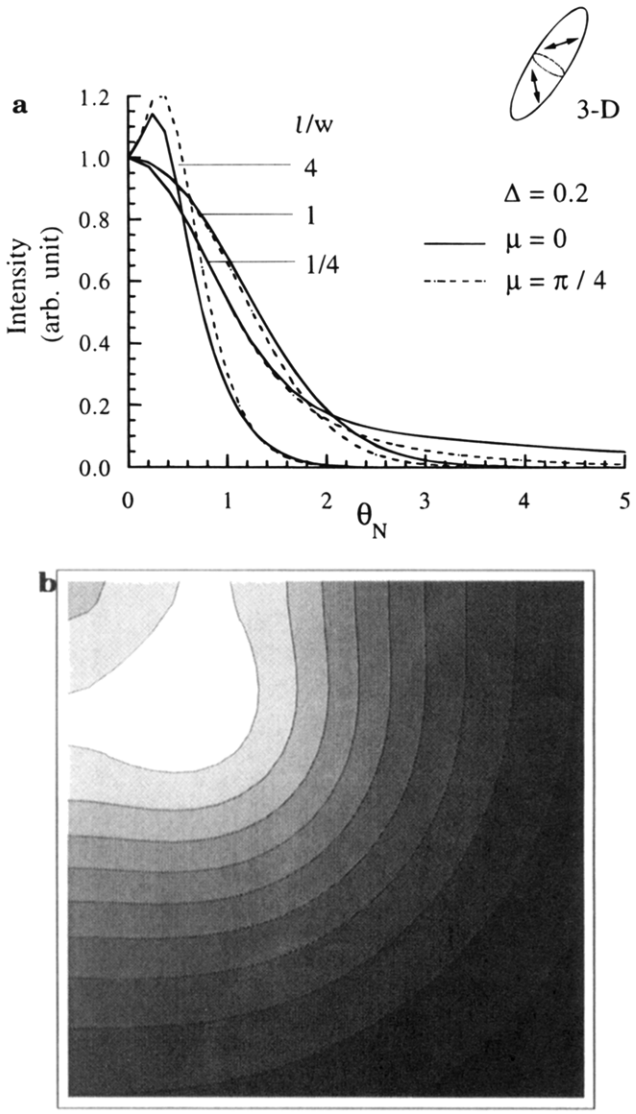

Figure 13. (a) Case 6: Scattered intensity. Two grains per CGP, full 3D averaging. Optic axes at ±45° to CGP axis. (b) Contour plot for $l/w = 4$. Full horizontal scale is $\theta_N = 1$. The incident beam is located in the upper left corner.

ously in diblock copolymers with cylindrical morphology. A logical extension of these studies is to attempt to apply these techniques and their interpretations to deformed block copolymers.

The cause of orientation correlations between adjacent grains in cylindrical-morphology diblock copolymers is not clear. Just after quenching from the disordered to the ordered state, one expects cylinders to grow with random orientations in different regions of the sample. Perhaps boundaries between grains with angles less than or greater than 90° anneal readily, leaving behind a greater proportion of grain boundaries in which the cylinders are perpendicular to each other. Studies of scattering patterns and microscopy as a function of annealing time may shed further light on the origin of the observed correlations.

Another point worth noting is that the lamellar system we previously studied[5,6] exhibited an azimuthally symmetric scattering pattern, with a maximum intensity in the forward direction. This suggests the absence of correlations between grains, as well as grains that are, on average, spherical in shape. In terms of our model calculations, this would correspond to one grain per CGP, with $l = w$. One possible explanation for this qualitative difference between lamellar and cylindrical systems is that the annealing of lamellar grains occurs either less readily or independently of lamellar orientation, giving rise to a random variety of defects and grain boundaries.

Acknowledgment. We thank the National Science Foundation for financial support [DMR-9457950]. We also thank Kalle Levon for use of his polarized light microscope and Richard Stein for illuminating discussions concerning correlations in random anisotropic media.

Appendix A. Determination of Coefficients for Specific CGP Geometries

For each CGP we have the geometry illustrated in Figure 7; $\mathbf{s}_0 = a_z$ is a unit vector in the incident direction, $\mathbf{s}$ is a unit vector in the scattered direction, $\mathbf{g}$ is a unit vector along the grain axis, $\mathbf{o}$ is a unit vector along the optic axis of grain. The relevant unit vectors are

$$\mathbf{s}_0 = \{0, 0, 1\}$$

$$\mathbf{s} = \{\sin[\theta]\sin[\mu], \sin[\theta]\cos[\mu], \cos[\theta]\}$$

$$\mathbf{g} = \{\sin[\theta_g]\sin[\mu_g], \sin[\theta_g]\cos[\mu_g], \cos[\theta_g]\} \quad \text{(A1)}$$

$$\mathbf{l} = \mathbf{s}_0 \times \mathbf{g}/|\mathbf{s}_0 \times \mathbf{g} \qquad \mathbf{m} = \mathbf{g} \times \mathbf{l}$$

($\mathbf{g}$, $\mathbf{l}$, $\mathbf{m}$ form unit Cartesian vectors)

$$\mathbf{o} = \cos[\theta_0]\,\mathbf{g} + \sin[\theta_0]\cos[\mu_0]\,\mathbf{l} + \sin[\theta_0]\sin[\mu_0]\,\mathbf{m}$$

Since

$$o_x = \sin(\theta_A)\sin(\mu_A)$$

$$o_y = \sin(\theta_A)\cos(\mu_A) \quad \text{(A2)}$$

we have for the optic axis dependent coefficients in eq 21

$$F_\alpha(\theta_g,\mu_g,\theta_{0_\alpha},\mu_{0_\alpha}) = \frac{1}{2}\sin^2(\theta_\alpha)\sin(2\mu_\alpha) = (o_\alpha)_x(o_\alpha)_y = (\cos\mu_g\cos\theta_0\sin\theta_g + \cos\mu_0\sin\mu_g\sin\theta_0 - \cos\mu_g\cos\theta_g\sin\mu_0\sin\theta_0)(\cos\theta_0\sin\mu_g\sin\theta_g - \cos\mu_g\cos\mu_0\sin\theta_0 - \cos\theta_g\sin\mu_g\sin\mu_0\sin\theta_0) \quad \text{(A3)}$$

Evaluating eq 21 for various assumed geometries leads to the corresponding a and b coefficients. The angular distribution of the intensity for each case then follows from eqs 26–29. Cases discussed in the text are described below.

(Case 1): Single grain per CGP, with the optic axis along the CGP axis $\{\theta_{0A} = 0, P_\mu(\mu_0) = 1/(2\pi)\}$.

$$a_{AA}[\theta_g] = \sin^4[\theta_g] \qquad b_{AA}[\theta_g] = -\sin^4[\theta_g]$$

$$a_{BB}[\theta_g] = 0 \qquad b_{BB}[\theta_g] = 0 \quad \text{(A4)}$$

$$a_{AB}[\theta_g] = 0 \qquad b_{AB}[\theta_g] = 0$$

(Case 2): Two grains per CGP, restricted two-dimensional problem. The plane of the CGP is perpendicular to the incident beam, and optic axes are in the plane of the CGP. Thus $P_\theta[\theta_g] = \delta(\theta_g - \pi/2)$, $P_\mu(\mu_0) = \delta(\mu_0)$. Mirror images about the CGP axis are included

in the statistical ensemble.

$$a_{AA}[\pi/2] = 1 \qquad b_{AA}[\pi/2] = -\cos[4\theta_{0A}]$$

$$a_{BB}[\pi/2] = 1 \qquad b_{BB}[\pi/2] = -\cos[4\theta_{0B}] \quad \text{(A5)}$$

$$a_{AB}[\pi/2] = \cos(2(\theta_{0A}-\theta_{0B})) \qquad b_{AB}[\pi/2] = -\cos(2(\theta_{0A}+\theta_{0B}))$$

Figure 10 illustrates the special case $\theta_{0A} = 0$, $\theta_{0B} = \pi/2$.

(Case 3): Two grains per CGP, unrestricted two-dimensional problem. The plane of the CGP is perpendicular to the incident beam, and the optic axes are not restricted to the plane of the CGP. $P_\theta[\theta_g] = \delta(\theta_g - \pi/2)$, $P_\mu(\mu_0) = 1/(2\pi)$. For the special case $\theta_{0A} = 0$, $\theta_{0B} = \pi/2$:

$$a_{AA}[\pi/2] = {}^1/_8 \qquad b_{AA}[\pi/2] = -{}^1/_8$$

$$a_{BB}[\pi/2] = {}^3/_{64} \qquad b_{BB}[\pi/2] = -{}^3/_{64} \quad \text{(A6)}$$

$$a_{AB}[\pi/2] = -{}^1/_{16} \qquad b_{AB}[\pi/2] = {}^1/_{16}$$

(Case 4): Three dimensions, two grains per CGP, $\theta_{0A} = 0$, $\theta_{0B} = \pi/2$.

$$a_{AA}(\theta_g) = \frac{1}{64}[3 - 4\cos[2\theta_g] + \cos[4\theta_g]]$$

$$b_{AA}(\theta_g) = \frac{1}{64}[-3 + 4\cos[2\theta_g] - \cos[4\theta_g]]$$

$$a_{BB}(\theta_g) = \frac{1}{512}[41 + 20\cos[2\theta_g] + 3\cos[4\theta_g]]$$

$$b_{BB}(\theta_g) = \frac{1}{512}[-9 + 12\cos[2\theta_g] - 3\cos[4\theta_g]] \quad \text{(A7)}$$

$$a_{AB}(\theta_g) = \frac{1}{128}[-3 + 4\cos[2\theta_g] - \cos[4\theta_g]]$$

$$b_{AB}(\theta_g) = \frac{1}{128}[3 - 4\cos[2\theta_g] + \cos[4\theta_g]]$$

(Case 5): Three dimensions, two grains per CGP, $\theta_{0A} = \pi/2$, $\theta_{0B} = \pi/2$, $\Delta\mu = \pi/2$.

$$a_{AA}(\theta_g) = a_{BB}(\theta_g) = \frac{1}{512}[41 + 20\cos[2\theta_g] + 3\cos[4\theta_g]]$$

$$b_{AA}(\theta_g) = b_{BB}(\theta_g) = \frac{1}{512}[-9 + 12\cos[2\theta_g] - 3\cos[4\theta_g]]$$

$$a_{AB}(\theta_g) = \frac{1}{512}[-29 - 36\cos[2\theta_g] + \cos[4\theta_g]] \quad \text{(A8)}$$

$$b_{AB}(\theta_g) = \frac{1}{512}[-3 + 4\cos[2\theta_g] - \cos[4\theta_g]]$$

(Case 6): Three dimensions, two grains per CGP, $\theta_{0A} = \pi/4$, $\theta_{0B} = 3\pi/4$, $\Delta\mu = 0$.

$$a_{AA}(\theta_g) = a_{BB}(\theta_g) = \frac{1}{2048}[121 - 44\cos[2\theta_g] - 13\cos[4\theta_g]]$$

$$b_{AA}(\theta_g) = b_{BB}(\theta_g) = \frac{1}{2048}[39 - 52\cos[2\theta_g] + 13\cos[4\theta_g]]$$

$$a_{AB}(\theta_g) = \frac{1}{2048}[-39 + 84\cos[2\theta_g] + 19\cos[4\theta_g]] \quad \text{(A9)}$$

$$b_{AB}(\theta_g) = \frac{1}{2048}[-57 + 76\cos[2\theta_g] - 19\cos[4\theta_g]]$$

References and Notes

(1) Bates, F. S.; Fredrickson, G. H. *Annu. Rev. Phys. Chem.* **1990**, *41*, 525.
(2) Gido, S. P.; Gunther, J.; Thomas, E. L.; Hoffman, D. *Macromolecules* **1993**, *26*, 2636.
(3) Kawasaki, K.; Onuki, A. *Phys. Rev. A* **1990**, *42*, 3664.
(4) Balsara, N. P.; Dai, H. J.; Kesani, P. K.; Garetz, B. A.; Hammouda, B. *Macromolecules* **1994**, *27*, 7406.
(5) Balsara, N. P.; Garetz, B. A.; Dai, H. J. *Macromolecules* **1992**, *25*, 6072.
(6) Garetz, B. A.; Newstein, M. C.; Dai, H. J.; Jonnalagadda, S. V.; Balsara, N. P. *Macromolecules* **1993**, *26*, 3151.
(7) Perahia, D.; Vacca, G.; Patel, S. S.; Dai, H. J.; Balsara, N. P. *Macromolecules* **1994**, *27*, 7645.
(8) Bragg, W. L.; Pippard, A. B. *Acta Crystallogr.* **1953**, *6*, 865.
(9) Stein, R. S.; Rhodes, M. B. *J. Appl. Phys.* **1960**, *31*, 1873.
(10) Hashimoto, T.; Nakai, A.; Shiwaku, T.; Hasegawa, H.; Rojstaczer, S.; Stein, R. S. *Macromolecules* **1989**, *22*, 422.
(11) Lin, C. C.; Jonnalagadda, S. V.; Kesani, P. K.; Dai, H. J.; Balsara, N. P. *Macromolecules* **1994**, *27*, 7769.
(12) Yan, N. X.; Labes, M. M.; Baek, S. G.; Magda, J. J. *Macromolecules* **1994**, *27*, 2784.
(13) Demus, D.; Richter, L.; Strzelecki, L. *Polymer* **1983**, *24*, 295.
(14) Campbell, D.; White, J. R. *Polymer Characterization, Physical Techniques*; Chapman and Hall: London, 1989.
(15) van Aartsen, J. J. *Eur. Polym. J.* **1970**, *6*, 1095.
(16) Murakami, Y.; Hayashi, N.; Hashimoto, T.; Kawai, H. *Polym. J.* **1973**, *4*, 452.
(17) Greco, F. *Macromolecules* **1989**, *22*, 4622.
(18) Stein, R. S. In *Electromagnetic Scattering*; Kerker, M., Ed.; Pergamon Press: Oxford, U.K., 1963; p 439.
(19) Stein, R. S.; Wilson, P. R. *J. Appl. Phys.* **1962**, *13*, 1914.
(20) van Aartsen, J. J. *J. Colloid Interface Sci.* **1972**, *39*, 583.
(21) Stein, R. S.; Erhardt, P.; van Aartsen, J. J.; Clough, S.; Rhodes, M. *J. Polym. Sci., Part C* **1966**, 1.
(22) van de Hulst, H. C. *Light Scattering by Small Particles*; Wiley: New York, 1957.

MA946268Q